Experimental and simulation studies of melting and freezing in porous glasses

M. Sliwinska–Bartkowiak [a], J. Gras [a], R. Sikorski [a], G. Dudziak [a],
R. Radhakrishnan [b] and K. E. Gubbins [b]

[a] Instytut Fizyki, Uniwersytet im Adama Mickiewicza,
Umultowska 85, 61-614 Poznan, Poland.

[b] Department of Chemical Engineering, North Carolina State University,
113 Riddick Labs, Raleigh, NC 27695, USA

We report both experimental measurements and molecular simulations of the melting and freezing behavior of simple fluids in porous media. The experimental studies are for nitrobenzene in controlled pore glass (CPG) and Vycor. Dielectric relaxation spectroscopy was used to determine melting points of bulk and confined nitrobenzene. Structural information about the different confined phases was obtained by measuring the rotational dielectric relaxation times. Monte Carlo simulations were used to determine the shift in the melting point, for a simple fluid in slit pores having both repulsive and attractive walls. A method for calculating the free energy of solids in pores based on order parameter formulation is presented. Qualitative comparison between experiment and simulation are made with respect to the shift in the freezing temperatures, structure of confined phases and hysteresis behavior.

1 Introduction

Freezing in porous media has been widely employed in the characterization of porous materials. In the method termed thermoporometry, the shift in freezing temperature of water is determined, and the pore size distribution is inferred from a thermodynamic analysis which is analogous to the use of Kelvin's equation for capillary condensation; such an analysis breaks down in the case of micropores as the limit of small and inhomogeneous systems demand a more rigorous statistical mechanical treatment. Important questions regarding melting and freezing in pores are the nature of the phase transition (first order vs. continuous, due to varied dimensionality), the direction of shift in the melting temperature, nature and origin of hysteresis, structural changes of the condensed phases in the restricted pore geometries, the effect on latent heats, etc. Answers to these questions warrant a rigorous study of the free energy surfaces as a function of the relevant thermodynamic variables.

A classical thermodynamic argument based on simple capillary theory determines the freezing temperature as the point at which the chemical potential of the solid core inside

the pore equals that of the surrounding fluid. This leads to the Gibbs–Thomson equation,

$$\frac{\Delta T_f}{T_{fb}} = \frac{T_f - T_{fb}}{T_{fb}} = -2\frac{(\gamma_{ws} - \gamma_{wl})\nu}{H\lambda_{fb}} \quad (1)$$

where T_{fb} is the bulk freezing temperature, γ_{ws} and γ_{wl} are the corresponding wall–solid and wall–fluid surface tensions, ν is the molar volume of the liquid, λ_{fb} is the latent heat of melting in the bulk and H is the pore width.

Experiments on freezing that have used porous silica glass as the confinement medium have always resulted in a decrease in the freezing temperature, T_f, as compared to the bulk [1,2]. In a subsequent molecular simulation study of the effect of confinement on freezing of simple fluids in slit pores by Miyahara and Gubbins [3], it was shown that T_f was strongly affected by the strength of the attractive forces between the fluid molecules and the pore walls. For repulsive or weakly attractive potentials, the shift in the freezing temperature ΔT_f was negative. For strongly attracting walls such as carbons, an *increase* in T_f was observed. Thus, Miyahara and Gubbins explained the disparate experimental trends on the direction of the shift in the freezing temperature and provided the connection to the Gibbs–Thomson equation. The predictions of Miyahara and Gubbins were confirmed by free energy studies, that calculated the thermodynamic freezing temperature in confined systems and established the order of the phase transition [4,5].

Radhakrishnan and co–workers [6] also studied the freezing of CCl_4 in activated carbon fibers (ACF) of uniform nano–scale structures, using Monte Carlo simulation and differential scanning calorimetry (DSC). Micro–porous activated carbon fibers serve as highly attractive adsorbents for simple non–polar molecules. The DSC experiments verified the predictions about the *increase* in T_f, and the molecular results were consistent with equation (1) for pore widths in the mesoporous range; they also explained the deviation from the linear behavior in the case of micropores.

In this paper we examine the effect of the fluid–wall potential on the free energy surface and the structure of the confined fluid. We make qualitative comparisons between simulated and experimental results, regarding the fluid structure and hysteresis behavior.

2 Methods

Dielectric relaxation spectroscopy: The relative permittivity of a medium, $\kappa^* = \kappa' - i\kappa''$, is in general a complex quantity whose real part κ' (also known as the dielectric constant) is associated with the increase in capacitance due to the introduction of the dielectric. The imaginary component κ'' is associated with mechanisms that contribute to energy dissipation in the system, due to viscous damping of the rotational motion of the dipolar molecules in alternating fields. The latter effect is frequency dependent. The experimental setup consisted of a parallel plate capacitor of empty capacitance $C_o = 4.2$ pF. The capacitance, C, and the tangent loss, $\tan(\delta)$, of the capacitor filled with nitrobenzene between the plates were measured using a Solartron 1260 gain impedance analyzer, in the frequency range 1 Hz – 10 MHz, for various temperatures. For the case of nitrobenzene in porous silica, the sample was introduced between the capacitor plates

as a suspension of 200 μm mesh porous silica particles in pure nitrobenzene.

$$\kappa' = \frac{C}{C_o};\ \kappa'' = \frac{\tan(\delta)}{\kappa'} \tag{2}$$

In equation (2), C is the capacitance, C_o is the capacitance without the dielectric and δ is the angle by which current leads the voltage. Nitrobenzene was confined in porous silica (CPG and VYCOR), of pore widths H = 50 nm to 4 nm at 1 atm. pressure. The freezing temperature in the bulk is 5.6 ^{o}C (the liquid freezes to a monoclinic crystal). $\kappa^* = \kappa' - i\kappa''$, the complex dielectric permittivity is measured as a function of temperature and frequency.

For an isolated dipole rotating under an oscillating electric field in a viscous medium, the Debye dispersion relation is derived using classical mechanics,

$$\kappa^* = \kappa'_\infty + \frac{\kappa'_s - \kappa'_\infty}{1 + i\omega\tau} \tag{3}$$

The dielectric constant is a natural choice of order parameter to study freezing of dipolar liquids, because of the large change in the orientational polarizability between the liquid and solid phases. The dielectric relaxation time was calculated by fitting the dispersion spectrum of the complex permittivity near resonance to the Debye model of orientational relaxation. In the Debye dispersion relation (equation (3)), ω is the frequency of the applied potential and τ is the orientational (rotational) relaxation time of a dipolar molecule. The subscript s refers to static permittivity (low frequency limit, when the dipoles have sufficient time to be in phase with the applied field). The subscript ∞ refers to the optical permittivity (high frequency limit) and is a measure of the induced component of the permittivity.

Simulation: We performed GCMC simulations of Lennard–Jones methane adsorbed in regular slit shaped pores of pore width $H = 7.5\sigma_{ff}$ and varying fluid–wall strengths. Here H is the distance separating the planes through the centers of the surface-layer carbon atoms on opposing pore walls. The interaction between the adsorbed fluid molecules is modeled using the Lennard–Jones (12,6) potential with size and energy parameters chosen to describe methane (σ_{ff} = 0.381 nm, ϵ_{ff}/k_B = 148.1 K). The fluid-wall interaction is modeled using a "10–4–3" Steele potential [8],

$$\phi_{fw}(z) = 2\pi\rho_w\epsilon_{fw}\sigma_{fw}^2\Delta\left[\frac{2}{5}\left(\frac{\sigma_{fw}}{z}\right)^{10} - \left(\frac{\sigma_{fw}}{z}\right)^4 - \left(\frac{\sigma_{fw}^4}{3\Delta(z+0.61\Delta)^3}\right)\right] \tag{4}$$

Here, the σ's and ϵ's are the size and energy parameters in the LJ potential, the subscripts f and w denote fluid and wall respectively, z is the coordinate perpendicular to the pore walls and k_B is the Boltzmann's constant. The fluid–wall interaction energy parameters corresponding to a graphite pore were taken from Ref. [8]. For a given pore width H, the total potential energy from both walls is given by,

$$\phi_{pore}(z) = \phi_{fw}(z) + \phi_{fw}(H - z) \tag{5}$$

The strength of the fluid wall interaction is determined by the parameter $\alpha = 2\pi\rho_w\epsilon_{fw}\sigma_{fw}^2\Delta$.

	Model	Type	α
1	Purely repulsive	Hard wall	0
2	Weakly attractive	Silica wall	0.76
3	Strongly attractive	Graphite wall	2.0

The simulation runs were performed in the grand canonical ensemble, fixing the chemical potential μ, the volume V of the pore and the temperature T. The system typically consisted of 600–700 adsorbed molecules. For the case of attractive pore-wall interaction, the adsorbed molecules formed seven layers parallel to the plane of the pore walls. A rectilinear simulation cell of $10\sigma_{ff}$ by $10\sigma_{ff}$ in the plane parallel to the pore walls was used, consistent with a cutoff of $5\sigma_{ff}$ for the fluid–fluid interaction. The simulation was set up such that insertion, deletion and displacement moves were attempted with equal probability, and the displacement step was adjusted to have a 50% probability of acceptance. Thermodynamic properties were averaged over 100–500 million individual Monte Carlo steps. The length of the simulation was adjusted such that a minimum of fifty times the average number of particles in the system would be inserted and deleted during a single simulation run.

Free energy method: The method relies on the calculation of the Landau free energy as a function of an effective bond orientational order parameter Φ, using GCMC simulations [5]. The Landau free energy is defined by,

$$\Lambda[\Phi] \;=\; -k_B T \,\ln(P[\Phi]) \;+\; \text{constant} \tag{6}$$

where $P[\Phi]$ is the probability of observing the system having an order parameter value between Φ and $\Phi + \delta\Phi$. The probability distribution function $P[\Phi]$ is calculated in a GCMC simulation as a histogram, with the help of umbrella sampling. The grand free energy Ω is then related to the Landau free energy by

$$\exp(-\beta\Omega) \;=\; \int d\Phi \,\exp(-\beta\Lambda[\Phi]) \tag{7}$$

The grand free energy at a particular temperature can be calculated by numerically integrating equation (7) over the order parameter space.

We use a two–dimensional order parameter to characterize the order in each of the molecular layers.

$$\Phi_j \;=\; \left| \frac{1}{N_b} \sum_{k=1}^{N_b} \exp(i6\theta_k) \right| \;=\; \left| \langle \exp(i6\theta_k) \rangle_j \right| \tag{8}$$

Φ_j measures the hexagonal bond order within each layer j. Each nearest neighbor bond has a particular orientation in the plane of the given layer, and is described by the polar coordinate θ. The index k runs over the total number of nearest neighbor bonds N_b in layer j. The overall order parameter Φ is an average of the hexagonal order in all the layers. We expect $\Phi_j = 0$ when layer j has the structure of a two–dimensional liquid, $\Phi_j = 1$ in the crystal phase and $0 < \Phi_j < 1$ in a orientationally ordered layer.

3 Results

Dielectric spectroscopy: The capacitance C and tangent loss $\tan(\delta)$ were measured as a function of frequency and temperature for bulk nitrobenzene and for nitrobenzene adsorbed in CPG and Vycor glass of different pore sizes ranging from 50 nm to 4.0 nm. The typical behavior of κ' vs. T is shown in Figure 1(a). For pure, bulk nitrobenzene, there was a sharp increase in κ' at $T = 5.6$ ^{o}C, corresponding to the melting point of the pure substance. For nitrobenzene confined in CPG, the sample is introduced as a suspension of nitrobenzene filled CPG particles in pure nitrobenzene, between the capacitor plates. Thus capacitance measurement yielded an effective value of the relative permittivity of the suspension of CPG in pure nitrobenzene. Thus κ' showed two sudden changes. The increase that depended on pore size was attributed to melting in the pores, while the increase at 5.6 ^{o}C corresponded to the bulk melting [7]. The shifts in the melting temperature are plotted against the reciprocal pore width in Figure 1(b) for nitrobenzene in CPG obtained using both DSC and dielectric spectroscopy (DS) measurements. The deviations from linearity, and hence from the Gibbs–Thomson equation are appreciable at pore widths as small as 4.0 nm.

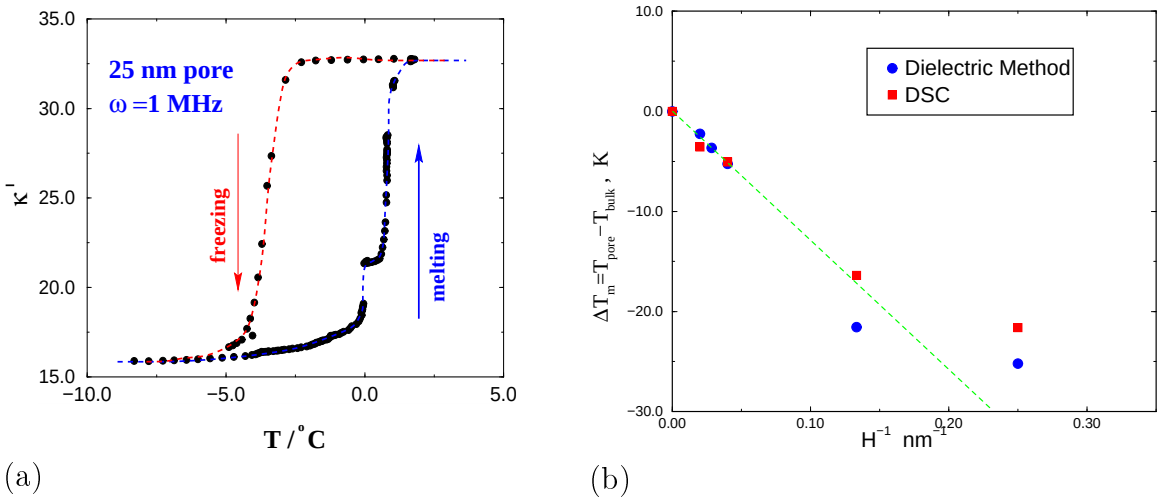

Figure 1. (a) Relative permittivity, κ', as a function of temperature, showing melting and freezing along with the hysteresis. (b) Shift in the melting temperature ΔT_m as a function of $1/H$ for nitrobenzene in CPG. The linear behavior is consistent with the Gibbs–Thomson equation.

The spectrum of the complex permittivity (κ', κ'' vs. ω) is fit to the dispersion relation (equation (3)), to determine the dielectric relaxation time τ, which gives valuable information about the structure of the condensed phase. The frequency range in this study is expected to encompass the resonant frequencies corresponding to the dielectric relaxation in the solid phases. To probe the liquid relaxation behavior would require a frequency range that is 4 to 5 orders of magnitude higher. The spectrum plots for nitrobenze in a 7.5 nm CPG at temperatures below the freezing temperature in the pore show a Debye type relaxation with a single time scale that is estimated to be $\tau = 1.44$ ms. At temperatures above the pore melting temperature, (e.g., see Figure 2 at $T = -4$ ^{o}C), the behavior

is significantly different. From the double peak structure of the $\kappa''(\omega)$ and the double inflection in the $\kappa'(\omega)$ curve, two different dielectric relaxation times are calculated. There is a shorter relaxation time $\tau_1 = 43.6\ \mu$s, in addition to the longer component $\tau_2 = 1.7$ ms. The longer component relaxation, $\tau_2 = 1.7$ ms, is attributed to the bulk crystalline phase of nitrobenzene. The shorter relaxation component, $\tau_1 = 43.6\ \mu$s, is attributed to the molecular dynamics of the contact layer.

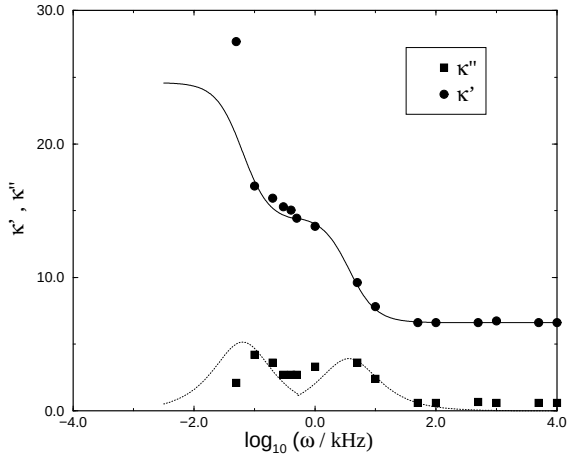

τ	Phase
$\tau_1 \sim 1.0$ ms	Crystal phase
$\tau_2 \sim 10.0\ \mu$s	Contact layer (liquid)
$\tau_{liquid} \sim 10^{-9}$s	Not measured here

Figure 2. Spectrum plot for nitrobenzene in a 7.5 nm pore at $T = -4\ ^o$C; this plot yields two distinct dielectric absorption regions. The solid and the dashed curves are fits to the Debye dispersion relation.

Simulation: The Landau free energy calculations showed that for the case of the hard walled and the silica walled pores, the freezing temperature in the pore was depressed compared to the bulk, while for the case of the graphite wall freezing temperature in the pore was greater than in the bulk [9]. This behavior is consistent with the trends observed in the literature and the Gibbs–Thomson equation. For the case of a hard wall pore, the confined system exists as either a liquid or a solid. For a weakly attractive pore that mimicks the silica interaction, the free energy surface in Figure 3(a) shows the presence of three phases. Phase A is the liquid phase and Phase C is the crystal phase. An intermediate phase B also exists, whose structure is plotted in Figure 3(b). The plots represent two–dimensional, in–plane pair correlation functions in each of the molecular layers. The pair correlation function of the contact layer (the layer adjacent to the pore walls) is isotropic, representing a liquid–like layer while the pair correlation functions for the inner layers show a broken translational symmetry corresponding to a 2–d crystalline phase; for this system the contact layers freeze at a temperature below that of the inner layers.

For a strongly attractive pore such as graphite, the free energy surface in Figure 4(a) also shows the presence of three phases. Phase A is the liquid phase and Phase C is the crystal phase. In this case the intermediate phase B has a different structure that is plotted in Figure 4(b); for this system the contact layers are crystalline while the inner layers are liquid–like. The contact layers freeze at a temperature higher than that of the inner layers.

The Landau free energy surfaces provide clear evidence of the existence of a contact layer with different structural properties compared to the pore interior, thereby supporting the experimental observation. The nature of the contact layer phase depends on the strength of the fluid–wall potential. For purely repulsive or mildly attractive pore-walls, the contact layer phase exists only as a metastable phase. As the strength of the fluid–wall attraction is increased, the contact layer phase becomes thermodynamically stable. Like the direction of shift in the freezing temperature, the structure of the contact layer phase also depends on the strength of the fluid wall interaction (i.e., whether the contact layer freezes before or after the rest of the inner layers).

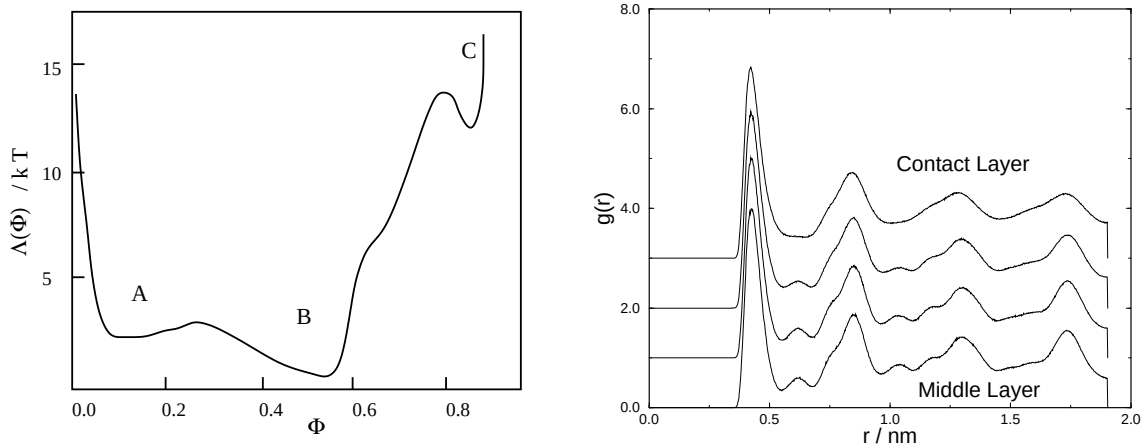

Figure 3. (a) The Landau free energy for methane confined in a model silica pore. The three minima correspond to three different phases. (b) The structure of phase B, showing that the contact layer is a fluid while the inner layers are frozen.

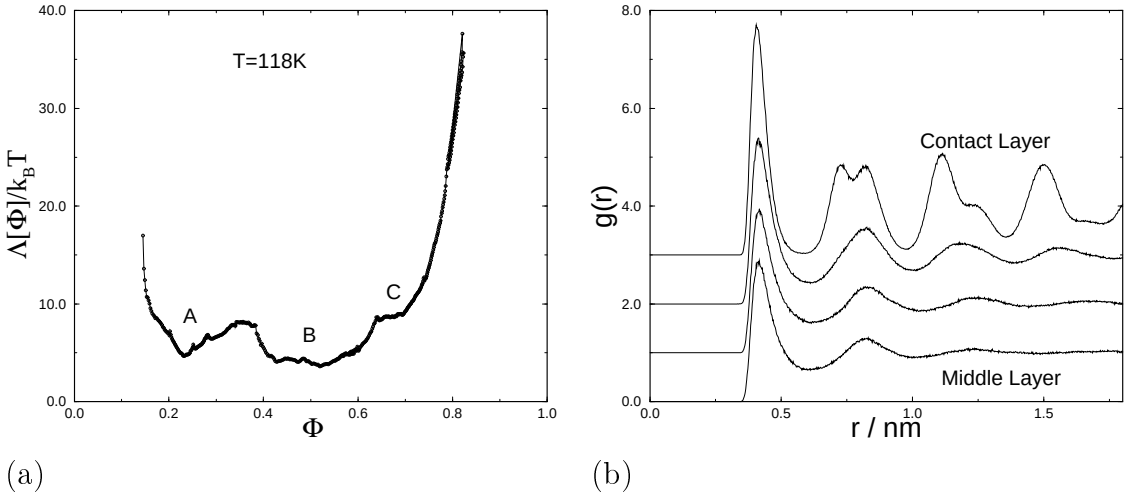

Figure 4. (a) The Landau free energy for methane confined in a model graphite pore. (b) The structure of phase B showing that the contact layer is frozen, while the inner layers remain fluid–like.

Hysteresis: Figure 1(a) shows κ' vs. T during melting and freezing and the hysteresis behavior in a 25 nm pore. The melting branch shows a step at $T = 0$ ^{o}C that is consistent with the melting of the contact layer. The second step at $T = 1$ ^{o}C corresponds to the melting of the inner layers in the pore, (a third increase at $T = 5.6$ ^{o}C corresponding to the bulk melting, is outside the range of the plot [7]). This behavior is consistent with the presence of the intermediate phase B with liquid–like contact layer; however, such a step is absent in the freezing branch. The asymmerty in the hysteresis behavior is explained by the Landau free energy curves. During melting, the system starts from the local minimum corresponding to the crystal phase in Figure 5(a), rolls over the barrier and gets trapped in the global minimum corresponding to the molten contact layer phase (this process is schematically represented by the arrow). The system jumps to the liquid phase at a lower temperature when the liquid phase becomes the thermodynamically stable phase. When the liquid freezes, however, the system starts at the local minimum corresponding to the liquid phase in Figure 5(b); as the system jumps over the barrier, it rides over the metastable minimum of the intermediate phase and gets trapped directly in the crystal phase. The behavior of the simple slit pore model is consistent with the real experimental system, which also suggests that the hysteresis behavior is due to metastable phases rather than kinetic factors.

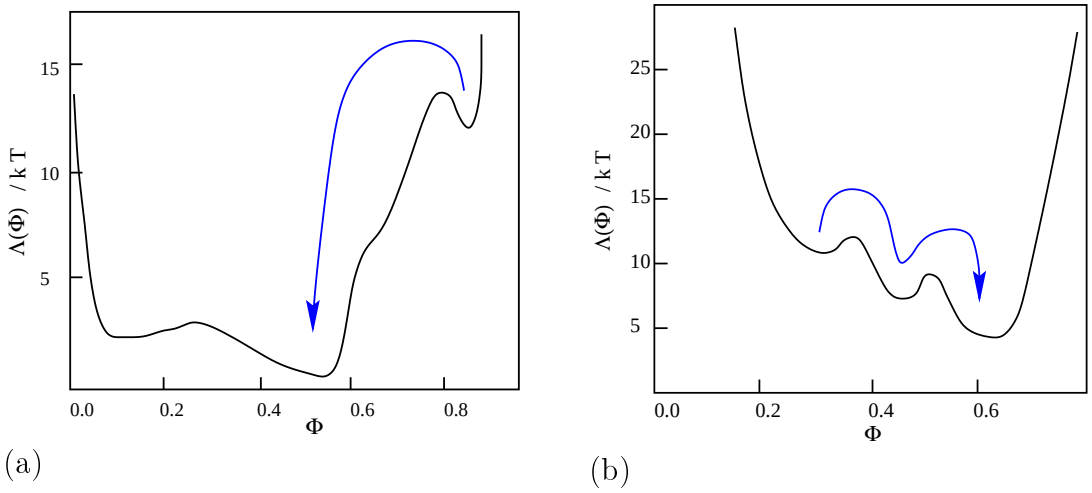

Figure 5. Landau free energy for methane in silica pore; (a) at 86 K, a temperature close to that where the crystal becomes unstable on heating; (b) at 80 K, a temperature close to that where the liquid phase becomes unstable on cooling.

4 Conclusions

The melting point of nitrobenzene in the pore is always depressed. The linear relationship between the shift in the pore melting temperature and the inverse pore diameter is consistent with the Gibbs–Thomson equation for larger pore sizes . The deviations from linearity, and hence from the Gibbs–Thomson equation are appreciable at pore widths as small as 4.0 nm. The quantitative estimates of the rotational relaxation times in the fluid and crystal phases of confined nitrobenzene support the existence of a contact layer with dynamic and structural properties different than the inner layers. The Landau free

energy calculation for the simple model that mimicked the weak silica wall interaction confirmed the existence of such a contact layer with different structural properties. The Gibbs–Thomson equation is valid when the effect of the contact layers are negligible on the inner layers. When the number of inner layers are comparable with the number of contact layers, a deviation from linear behavior (G-T regime) is observed. The freezing temperature in the "non-linear" regime is influenced by the freezing of the contact layers [6].

A systematic study of the influence of the strength of the fluid–wall interaction parameter α revealed that, for $\alpha < 0.5$, the intermediate phase B remains metastable for all temperatures. For the range $0.5 < \alpha < 1.2$, phase B becomes thermodynamically stable with the contact layer freezing at a temperature below that of the inner layers and for $\alpha > 1.6$, phase B becomes thermodynamically stable with the contact layer freezing at a temperature above that of the the inner layers [9].

The comparison of the hysteresis behavior in simulation and experiment, shows that the hysteresis is mainly due to the existence of metastable states rather than due to kinetic effects. The asymmetry in the freezing and melting branches of the adsorption curve is explained based on the Landau free energy surfaces. The Landau free energy approach is a powerful tool in determining the freezing temperature, nature of the phase transition, structure of the confined phases, existence of metastable states and origin of the hysteresis behavior.

Efforts are underway to use more realistic fluid potentials and pore models in the simulation. Recently Gelb and Gubbins [10] proposed a novel mechanism to realistically model porous silica glasses using spinodal decomposition of a binary fluid mixture in the two–phase liquid–liquid region. This model is known to closely represent the actual pore size distribution of real porous silica, and incorporates complex pore networking. We plan to study freezing of simple fluids using the free energy method in such a pore model, and to quantitatively compare with the experimental results for CCl_4 in CPG.

It is a pleasure to thank Katsumi Kaneko for helpful discussions. R.R thanks Adama Mickiewicz University, Poznan, Poland for their hospitality during a visit in the summer of 1998, when this work was carried out. This work was supported by grants from the National Science Foundation (Grant No. CTS–9896195) and KBN (Grant No. 2 PO3B 175 08), and by a grant from the U.S.–Poland Maria Sklodowska–Curie Joint fund (grant no. MEN/DOE–97–314). Supercomputer time was provided under a NSF/NRAC grant (MCA93S011).

5 References

1. Warnock J., Awschalom D.D., M.W. Shafer, Phys. Rev. Lett., 1986, 57(14), 1753.

2. Unruh K.M., Huber T.E., Huber C.A., Phys. Rev. B, 1993, 48(12), 9021.

3. Miyahara M., Gubbins K.E., J. Chem. Phys., 1997, 106(7), 2865.

4. Dominguez H., Allen M.P., Evans R., Mol. Phys., 1999, 96, 209.

5. Radhakrishnan R., Gubbins K.E., Mol. Phys., 1999, 96, 1249.

6. Radhakrishnan R, Gubbins KE, Watanabe A, Kaneko K, 1999, submitted to J. Chem. Phys.

7. Sliwinska–Bartkowiak M., Gras J., Sikorski R., Radhakrishnan R., Gelb L.D. and Gubbins K.E., Langmuir, 1999 (in press).

8. W.A. Steele, 1973, Surf. Sci. 36, 317.

9. Radhakrishnan R, Gubbins KE, M. Sliwinska-Bartkowiak, 1999, to be submitted to J. Chem. Phys.

10. Gelb L.D., Gubbins K.E., Langmuir, 1998, 14, 2097.